Engineered Science
DOI: https://dx.doi.org/10.30919/es8e801

Cold Plate Temperature Effect on Droplet and Frost Crystal Behaviors at the Early Condensation Frosting Stage Considering Plate Edge Effect

Long Zhang,[1] Mengjie Song,[1,*] Tianzhuo Zhan,[2] Jun Shen[1] and Chaobin Dang[3,*]

Abstract

The condensation frosting phenomenon commonly exists in engineering applications, and the relevant studies on flat plates with fixed surface temperatures are the most concerned in related fields. The existing studies usually focus on droplet condensation and frozen characteristics in the center region of cold plates and cannot reveal those near the plate edge. Therefore, a systematic study from droplet condensation to frost layer growth stages in the edge region of a cold plate was conducted in this paper. The experimental results showed that the frozen stage period of the edge-affected zone was significantly smaller than that of the unaffected zone. The ratio of average freezing wave propagation velocity in the edge-affected zone to that in the unaffected zone at plate temperatures of -9.0, -14.0, and -19.0 °C were 7.70, 5.56, and 5.11, respectively. Besides, the area-average equivalent diameter and coverage area ratio of droplets decreased with a decrease in plate temperature at the end of their respective droplet frozen stages. This study may help to better understand temporal and spatial condensation frosting characteristics on a horizontal cold plate with right-angle edges, and guide the establishment of a staged and divisional frosting model on cold plates.

Keywords: Frosting characteristic; Stage division; Plate temperature; Edge effect; Frost surface roughness.
Received: 26 August 2022; Revised: 19 November 2022; Accepted: 29 November 2022.
Article type: Research article.

1. Introduction

Frosting widely occurs in many fields of human production and life, such as meteorology,[1] transportation[2] electric power communication,[3] and energy application.[4] In most of these fields, frosting usually brings negative impacts, especially in engineering applications. For example, frost may increase air side thermal resistance and pressure drop of the outdoor coil for an air source heat pump, which significantly worsens its heating performance.[5,6] Similarly, frost may also block the air passages of the evaporator for a refrigerator and reduce its cooling capacity and efficiency.[7] In general, investigating the frosting mechanism and characteristic in depth is the primary task to resolve the frosting problem. From the perspective of avoiding or delaying frosting, it is necessary to better understand the influencing factors of frosting and the corresponding action mechanisms.[8] From the perspective of defrosting, a better understanding of frost property parameters and distribution characteristics can help to optimize the system control strategy.[9,10] Therefore, frosting mechanism and characteristic is consistently a hot topic in the relevant research fields.

In general, frosting type can be divided into condensation frosting and de-sublimation frosting based on the frosting mechanism. Since the de-sublimation frosting mainly occurs at an ultra-low surface temperature.[11] or water vapor pressure,[12] condensation frosting is much more common in engineering applications. Besides, it is difficult to quantitatively investigate the condensation frosting characteristics on most of the frosting components in practical applications due to their complex structures. Therefore, the

[1] *Department of Energy and Power Engineering, School of Mechanical Engineering, Beijing Institute of Technology, Beijing 100081, China.*
[2] *Graduate School of Interdisciplinary New Science, Toyo University, 2100 Kujirai, Kawagoe, Saitama 350-8585, Japan.*
[3] *Graduate School of Engineering, University of Fukui, 3-9-1 Bunkyo, Fukui-shi, Fukui 910-8507, Japan.*
[*] *E-mail:* mengjie.song@gmail.com (M. Song), dangcb@u-fukui.ac.jp (C. Dang)

majority of relevant studies focused on condensation frosting characteristics on cold surfaces with simple structures, which are also elements of complex frosting components.[13] These simple structures may be divided into five types, including flat plates with fixed surface temperatures, flat plates with fixed base temperatures, columns, parallel flat plates, and a set of fins. For the latter four simple structures with uneven surface temperatures or air side parameters, the relevant studies mainly focused on their frost distribution characteristics. For example, Kwon *et al*.[14] found that the frost layer was not completely symmetric distribution based on the center base of a flat plate but slightly thicker at its air side entrance. For a round tube, Ramirez-Hernandez *et al*.[15] indicated that frost layer was thicker around its windward side, and the difference in frost layer thickness between windward and leeward sides decreased with an increase in Reynolds number. For a horizontal parallel plate, Nascimento *et al*.[16] experimentally demonstrated that frost layer thickness was fairly uniform along its air flow direction. For a set of fins, Wu *et al*.[17] suggested that frost layer thickness was thicker at the air side entrance and fin base and the amount of frost on windward fins was greater than that on leeward fins.

Compared to the aforementioned simple structures, a flat plate with fixed surface temperature was simpler and easier to reveal condensation frosting mechanisms. Therefore, the relevant studies on flat plates with fixed surface temperatures were also the most concerned.[13] Overall, these studies may be classified based on the influencing factors of frosting, such as air side frosting conditions, electric and magnetic fields, plate inclination, plate surface treatment, and plate temperature. With respect to air side frosting conditions, air temperature, relative humidity, velocity, and fine particulate matter are considered. In general, frost thickness could be larger when the air relative humidity and velocity are higher. Frost density could be larger when the air temperature and velocity are higher.[18] For frost thickness, it was smaller when the air temperature was higher in most of the relevant studies, but an opposite trend can be found in studies conducted by Cheng and Shiu[19] and Wang *et al*..[20] For frost density, contrary conclusions can be found in studies conducted by Hermes *et al*.[21] and Lee and Ro.[22] Besides, fine particulate matter with a diameter of 2.5 μm or less may accelerate heterogeneous nucleation and hence promote frost growth.[23] For the electric field, Tudor and Ohadi[24] found that a constant alternating current field may accelerate frost growth but a sweeping alternating current field effectively reduce frost amount by up to 46%. Besides, employing a magnetic field can also effectively restrain frost growth by reducing the growth rate of droplets and delaying droplet solidification[25]. For the plate inclination, the gravity effect on condensed droplets may be increased with the increased inclination angle of the plate. The related experimental results showed that the increased gravity effect could help to prevent condensed droplets from merging, and increase frost thickness but decrease frost density.[26,27] For the plate surface treatment, condensation frost growth may be delayed due to the increased nucleation energy barrier and the condensed droplets were more scattered as surface contact angle increased.[28,29]

Concerning the plate temperature, as the basic inducement for the condensation frosting process, the relevant studies were paid more attention. At the droplet condensation stage, critical Gibbs free energy for water vapor condenses as stable droplets decreased with a decrease in plate temperature. As a result, droplet distribution density and radius increased with a decrease in plate temperature.[30] Besides, droplet behavior such as coalescence and jumping can be observed, especially on hydrophobic surfaces.[31] It is noted that these droplets were supercooled during this stage and the onset time of freezing decreased with a decrease in plate temperature.[32] At the droplet frozen stage, apart from the solidification of a single droplet,[33], a notable phenomenon defined as freezing wave propagation was reported by some researchers.[34,35] The freezing wave propagation increased with a decrease in plate temperature.[36] At the frost layer growth stage, frost crystal morphology was significantly affected by plate temperature. It usually changed from column to needle, sheath, sector, and feather with a decrease in plate temperature.[37] For frost thickness and frost surface roughness, they both increased with a decrease in plate temperature at this stage on horizontal and vertical cold plates.[38,39] At the frost fully growth stage, fluctuation in frost thickness due to reverse melting can be observed. In general, it can be noted that most of the existing droplet condensation and frozen characteristics can only reveal those in the center region of cold plates while ignoring the plate edge effect. However, the plate edge usually acts as an initial nucleation site for droplet condensation and frozen.[35] The droplet condensation and frozen characteristics in the edge region of cold plates should be further investigated. Besides, frost thickness and surface roughness were mainly obtained in terms of the frost layer in the edge region of cold plates. Therefore, a systematic study should be carried out from droplet condensation to frost layer growth stages in the edge region of a cold plate.

Accordingly, in this study, the effects of cold plate temperature on droplet and frost layer growth characteristics at the early condensation frosting stage considering the plate edge effect are experimentally investigated. This paper first gives descriptions of a specific experimental setup, procedure,

and conditions, as well as data reductions. Thereafter, qualitative and quantitative analysis of the cold plate temperature effect coupled with its edge effect on droplet behavior, size and distribution characteristics, and frost crystal behavior and frost layer growth characteristics are both presented in detail. Finally, conclusions are provided. This study may help to better understand temporal and spatial condensation frosting characteristics on a horizontal cold plate with a sharp edge, and guide the establishment of a staged and divisional frosting model on cold plates. Moreover, this study may also provide new insights into delaying frosting based on the plate edge effect.

2. Methodology

2.1 Experimental setup

To facilitate the objective of this study, a specific experimental setup was constructed, as shown in Fig. 1. The setup consisted of an air conditioning system, air duct system, nitrogen protection system, visualization system, and cold plate temperature control system. The air conditioning system mainly included a filter, variable speed air fan, air cooler, electric heater, and humidifier, and can provide air flow at a given temperature, relative humidity, and velocity. For the air duct system, it was comprised of air ducts with thermal insulation, an equalizer to realize even air distribution, and acrylic plates in the test region for the convenience of observing frosted cold plate. The nitrogen protection system was comprised of a nitrogen mask and nitrogen pipe connecting with the nitrogen gas tank, which can avoid droplet condensation at the cooling stage of the experimental cold plate. The visualization system was mainly comprised of two cameras and a cold light source. In particular, one camera was used for observing the cold plate from a top view and the other from a side view.

For the cold plate temperature control system, it was mainly comprised of a horizontal copper plate, thermoelectric module, and heat exchanger. The thermoelectric module was used for cooling the copper plate temperature and the heat exchanger for taking away the heat from the thermoelectric module. Besides, thermal grease was used for attaching the aforementioned components closely and four thermocouples were uniformly attached at the bottom of the copper plate to measure its temperature. Considering that the thermal conductivity of the experimental copper plate was 401 W/(m·k) and its thickness was 2 mm, the temperature between its upper and lower surface was less than 0.1 °C. Accordingly, these thermocouples can be used for evaluating the surface temperature of the copper plate. In terms of thermocouples, a proportional integral derivative temperature controller has been employed to control the thermoelectric module. The surface temperature of the copper plate can be maintained at the designated values with a deviation of ±0.2 °C.

The details of the experimental copper plate can be found in Fig. 2. As seen, the dimensions of the experimental copper plate were 40 mm × 40 mm × 2 mm, and that of the field of view by the top view camera was 2600 μm × 1400 μm, respectively. Besides, the wettability of the experimental copper plate was hydrophilic, and the copper plate was polished with sandpapers (P800) to eliminate obvious defects.

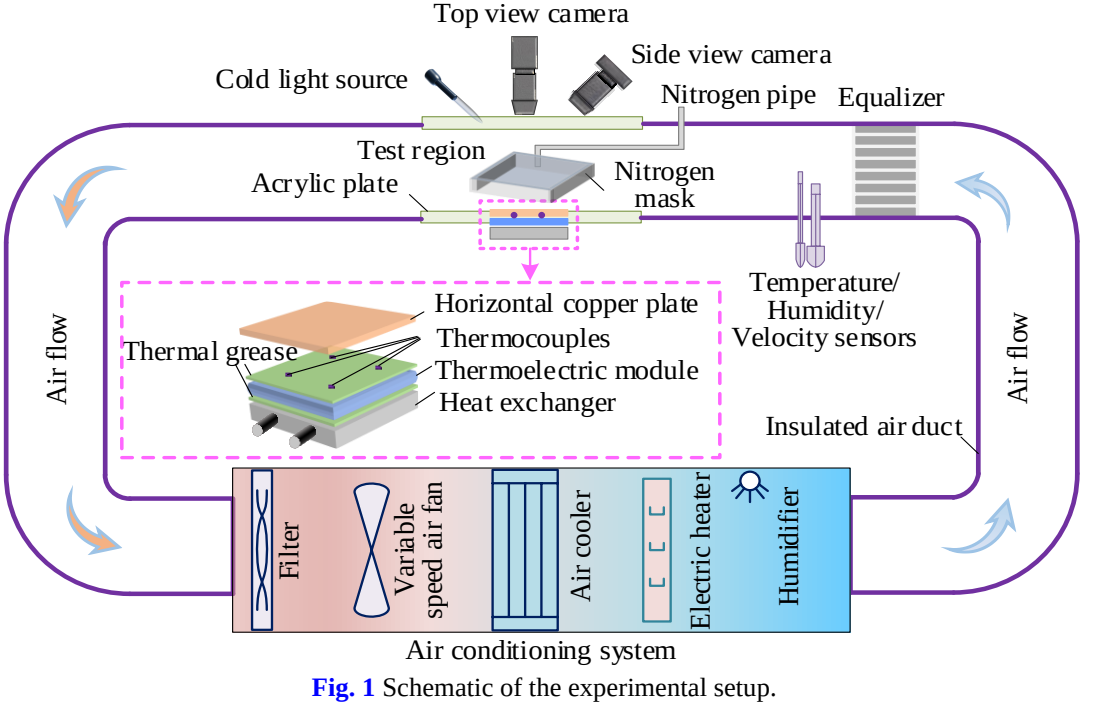

Fig. 1 Schematic of the experimental setup.

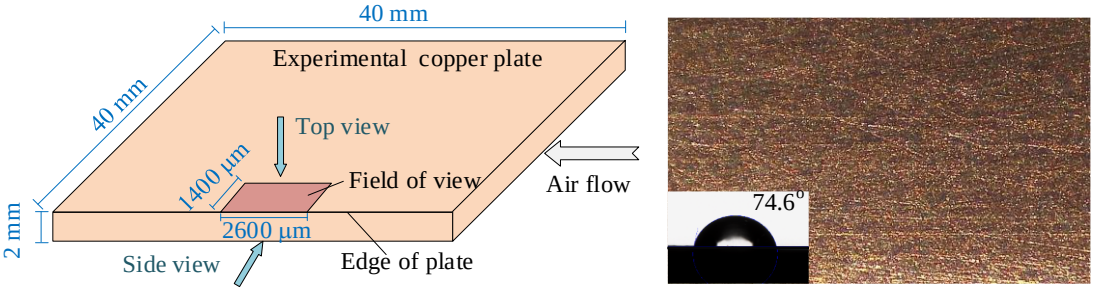

(a) Schematic of field of view (b) Photo of contact angle

Fig. 2 Schematic of the field of view on the experimental plate and its contact angle.

Therefore, the uniformity of surface characteristics of the experimental copper plate was good. The average values of the contact angle, advancing angle, receding angle and contact angle hysteresis for the experimental copper plate front and side surfaces were 74.6° ± 2.2°, 93.2° ± 3.1°, 60.3° ± 2.8°, and 32.9° ± 3.0°, respectively. The specifications of the corresponding experimental measuring instruments are shown in Table 1.

Table 1. Specifications of the corresponding experimental measuring instruments.

No.	Item	Type	Accuracy
1	Air temperature	T-TT-36	± 0.15 °C
2	Air relative humidity sensor	Rotronic HF320	± 2%
3	Air velocity sensor	EE650	± 0.2 m/s
4	Cold plate temperature	T-TT-36	± 0.15 °C
5	Top view camera	CCD AO-508U	Resolution of 2592 × 1944
6	Side view camera	Canon-60D	Resolution of 1920 × 1080
7	Contact angle meter	ASR-709B	± 0.1°

2.2 Experimental procedure and conditions

Before each condensation frosting experiment, the following two steps of preparation were necessary. The first step was to adjust air side frosting conditions by the air conditioning system and maintained the temperature, relative humidity, and velocity of air flow passing through the experimental plate at given values. The second step was to adjust the cold plate temperature and maintained it at a given value. To avoid droplet condensation on the experimental plate at this stage, the plate was covered by a mask filled with nitrogen by connecting it to a high-pressure nitrogen tank. Thereafter, the condensation frosting experiment started with removing the nitrogen mask. The experimental conditions were designed referring to literature reviews carried out by Zhang *et al*.[13] and Song and Dang,[40] as shown in Table 2. As seen, there was a total of five cases in this study, and the only difference among them was the plate temperature. It can be noted that the plate temperature was not uniformly spaced. This was because a significant variation in frosting characteristics occurred before and after -9.0 °C, which will be presented in detail in Section 3. The air temperature, relative humidity, dew point temperature, velocity, and frosting time were 20.0 °C, 50%, 9.3 °C, 1.5 m/s, and 1,200 s, respectively, for all cases.

2.3 Data reductions

To better quantitatively investigate frosting characteristics at the early condensation frosting stage, three sub-stages can be divided, as shown in Fig. 3. The first is the condensation stage, during which water vapor in air nucleates on the cold plate surface and gradually grows as small droplets. In particular, droplet coalescence may occur when droplets continue to grow and touch each other. The second is the frozen stage, during which droplets freeze and freezing wave propagation can be observed. The onset of freezing is the time point when a frozen phenomenon first occurs in the field of view, while

Table 2. Experimental conditions.

Case	Plate temperature (°C)	Air temperature (°C)	Air relative humidity (-)	Air dew point temperature (°C)	Air velocity (m/s)	Frosting time (s)
1	-5.0					
2	-8.0					
3	-9.0	20.0	50%	9.3	1.5	1,200
4	-14.0					
5	-19.0					

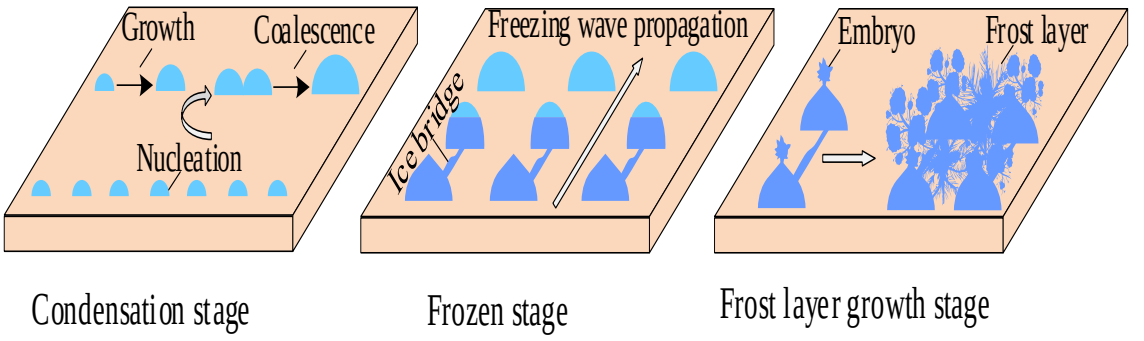

Fig. 3 Schematic of the sub-stage division at the early condensation frosting stage.

the termination of freezing is when the last droplet in the field of view solidifies. In general, there are three modes of freezing wave propagation. In 2013, Guadarrama-Cetina first proposed that the freezing wave was mainly propagated by ice bridges, which grew from frozen droplets to liquid droplets.[41] The similar phenomenon has been demonstrated in many other studies in terms of cold plates with different surface characteristics.[42-44] Apart from ice bridges, frost halo[45] and freezing rain[46] have also been demonstrated as other ways of propagation mechanisms. The last is the frost layer growth stage, during which embryos first grow at the tops of droplets, and then frost crystals grow three-dimensional. The intertwined frost crystals form a layer of frost, which as a whole mainly grow vertically to the cold surface.

In general, droplets close to the plate edge may be significantly larger than others due to the edge effect for regular plates without droplet jumping. The edge effect is mainly caused by the following two reasons. The first is that there may be more defects existing in the plate edge which may lower the energy barrier of nucleation. The second is that the heat and mass transfer rates near the plate edge may be larger than other zones due to its geometric singularity. Therefore, to better quantitatively investigate the plate edge effect on the condensation frosting characteristics, the droplets on the cold plate were further divided, as shown in Fig. 4. In this study, the single row of larger droplets close to the plate edge was defined as edge-affected droplets and the remained droplets as unaffected droplets. Accordingly, the cold plate was also further divided into an edge-affected zone and an unaffected zone based on droplet division. It can be noted that the edge-affected zone may be greater as the edge-affected droplets got larger as time passed.

Based on the photos captured by the top view camera, droplet size and distribution parameters during droplet condensation and frozen stages can be evaluated. It was noted that the droplets whose diameters were less than 20 μm were ignored in this study due to the resolution limit of the top view camera. Based on the droplet morphology characteristic on a hydrophilic surface, the coverage area of a droplet in this study was evaluated by equation (1) as follows:

$$A_w = N_{p,in} \times A_p \tag{1}$$

where $N_{p,in}$ was the number of pixels covered by a droplet, and A_p the area of a pixel.

The area-average equivalent diameter of droplets[47] was evaluated by equation (2) as follows:

$$\bar{D}_w = \sqrt{\frac{4\sum_{i=1}^{N_w} A_{w,i}}{\pi N_w}} \tag{2}$$

where N_w was the number of droplets.

The coverage area ratio of droplets to the corresponding zone can be evaluated by equation (3) as follows:

$$R_A = \frac{\sum_{i=1}^{N_w} A_{w,i}}{A_s} \tag{3}$$

where A_s was the corresponding zone area.

During the droplet frozen stage, the average freezing wave propagation velocity was evaluated by equation (4) as follows:

$$v_{fw} = \frac{L}{\Delta t} \tag{4}$$

where L was the equivalent distance in the corresponding zone, and Δt the frozen stage period in the corresponding zone.

Based on the photos captured by the side view cameras, the following droplet size and frost layer growth parameters can be evaluated:

The average droplet height during droplet condensation and frozen stages was evaluated by equation (5) as follows:

$$\bar{H}_w = \sqrt{\frac{\sum_{i=1}^{N_w} H_{w,i}}{N_w}} \tag{5}$$

where H_w was the height of a droplet.

The average frost layer thickness during frost layer growth stage was evaluated by equation (6) as follows:

$$\bar{\delta}_f = \frac{A_f}{L'} \tag{6}$$

where A_f was the area of the frost layer measured by the side

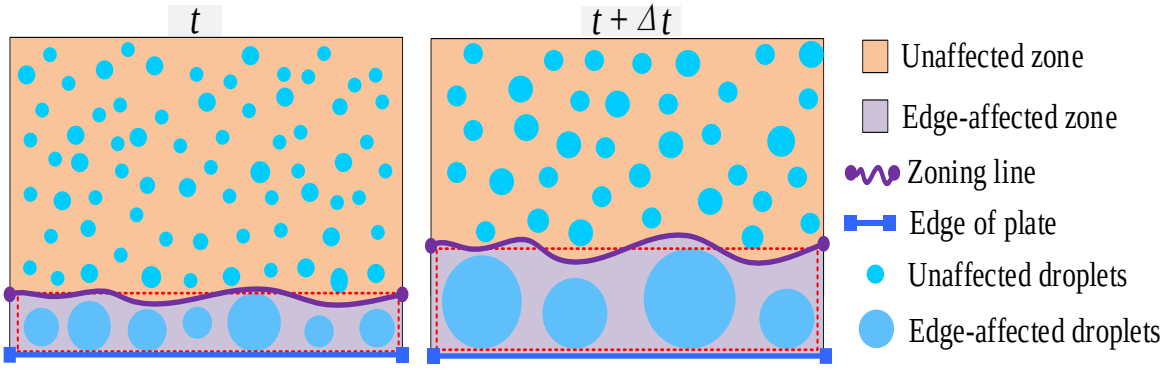

Fig. 4 Schematic of zone division for edge-affected and unaffected droplets.

view camera, and L' the length of the edge zone.

Based on the average frost layer thickness, the frost layer growth rate was evaluated by equation (7) as follows:

$$g_f = \frac{\bar{\delta}_f(t+\Delta t')-\bar{\delta}_f(t)}{\Delta t'} \quad (7)$$

where $\Delta t'$ was the time interval used for measuring frost thickness.

The frost layer surface roughness[48] was evaluated by equation (8) as follows:

$$RMS_f = \sqrt{\frac{\sum_{i=1}^{N_{sp}} (\delta_{f,i}-\bar{\delta}_f)^2}{N_{sp}}} \quad (8)$$

where N_{sp} was the number of sampling points, $\delta_{f,i}$ the local frost layer thickness of the sampling points.

The uncertainties of the aforementioned parameters can be evaluated using the error propagation formula presented by Rasul *et al.*.[49] For example, the uncertainty of the frost layer surface roughness was evaluated by equation (9) as follows:

$$u_{RMS_f} = \frac{\sqrt{\sum_{i=1}^{N_{sp}} \left(\frac{\partial RMS_f}{\partial(\delta_{f,i}-\bar{\delta}_f)} u_{(\delta_{f,i}-\bar{\delta}_f)} \times (\delta_{f,i}-\bar{\delta}_f) \right)^2}}{RMS_f} \quad (9)$$

In this study, the uncertainties of the area-average equivalent diameter of droplets, the coverage area ratio of droplets, the average height of droplets, frost layer thickness, frost layer growth rate, and frost layer surface roughness were ± 2.4%, ± 1.1%, ± 2.8%, ± 3.7%, ± 2.9%, and ± 2.2%, respectively.

3. Results and discussion

3.1 Analysis of droplet behaviors

Generally, frosting phenomenon exists when the cold surface temperature is lower than the dew-point temperature of ambient air and lower than the triple-point temperature of the water. In this study, the plate temperatures in all cases satisfied the frosting conditions, but different phenomena can be observed. As shown in Fig. 5, for Cases 1 and 2, droplets on the cold plate surface continued to grow up and did not freeze during the entire 1,200-s frosting period. Although the plate temperatures were lower than the triple point temperature of water, these droplets consistently exist in a subcooled state. This was because the supercooling degree of droplets was not large enough to overcome the energy barrier of nucleation. Obviously, the droplets were much larger when the plate temperature was lower from -5.0 to -8.0 °C due to the higher supercooling degree between the air stream and cold plate. When the plate temperature was lowered to -9.0 °C, droplet frozen phenomenon could be observed.

For Cases 3 to 5, it can be found that the onset time of freezing was advanced with a decrease in plate temperature. The onset time of freezing were 351, 108, and 42 s when the plate temperatures were -9.0, -14.0, and -19.0 °C, respectively. Besides, a significant difference in droplet size and distribution can be observed between the edge-affected zone and unaffected zone, which were defined in Section 2.3. In particular, all the droplet frozen phenomena occurred firstly in droplets near the plate edge, as indicated by the red circles in photos of Cases 3 to 5. This was because the energy barrier of nucleation near the plate edge was the lowest due to that more defects may be formed in this zone. The heterogeneous nucleation energy barrier[50] can be evaluated by equation (10) as follows:

$$\Delta G_c = \frac{4\pi}{3} \left(\frac{2\sigma_{vl}}{\rho_l R_w T_v \ln(\frac{p_v}{p_s})} \right)^2 \sigma_{vl} f(\theta) \quad (10)$$

where σ_{lv} was the interfacial free energy between vapor and liquid, and ρ_l the liquid water density, R_w the gas constant for water vapor, T_v the vapor temperature, p_v the vapor partial pressure of the humid air, p_s the saturated vapor pressure at the cold plate temperature, $f(\theta)$ the function which indicated the effect of the surface contact angle on the nucleation energy barrier, as evaluated by equation (11) as follows:

$$f(\theta) = \frac{(2+\cos\theta)(1-\cos\theta)^2}{4} \quad (11)$$

where θ was the surface contact angle.

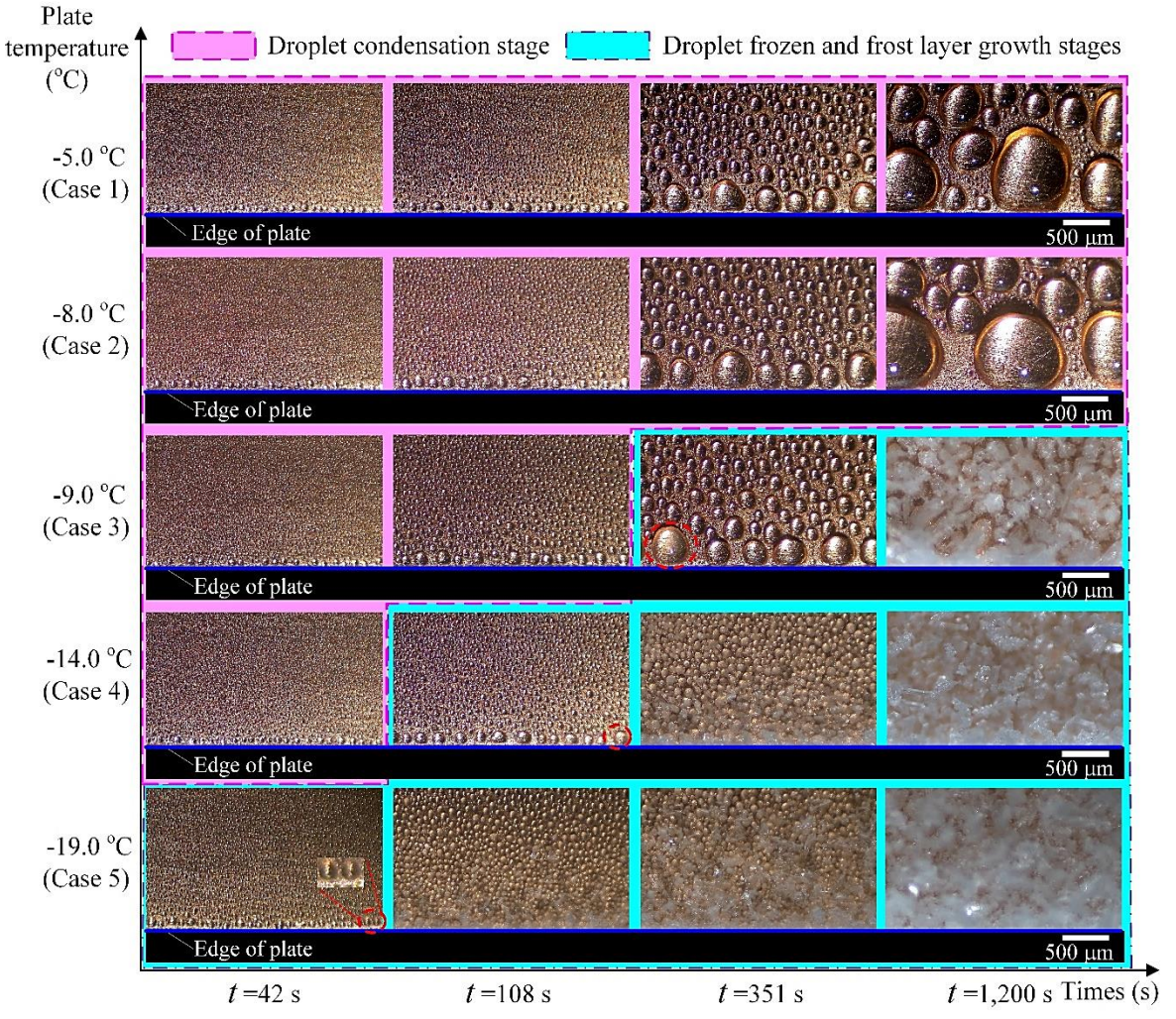

Fig. 5 Photos of droplets condensation, frozen and frost layer growth stages.

It should be noted that $f(\theta)$ increased with an increase in θ. For the experimental cold plate, defects could lower its surface contact angle and hence the value of $f(\theta)$. As a result, the energy barrier of nucleation near the plate edge was the lowest. More detailed differences in droplet size and distribution characteristics caused by the edge effect will be presented in Section 3.2.

During the droplet condensation stage, droplet coalescence phenomenon occurs when two or more droplets touch each other. For droplets near the plate edge, the droplet coalescence phenomenon not only occurred between droplets that were located on the same surface but also on two adjacent surfaces. As shown in Fig. 6(a), droplets A, C, and D were located on the front surface of cold plate, while droplet B on the side surface of cold plate. As droplets continued to grow up, droplets A and B coalesced and formed a new droplet E, while droplets C and D coalesced and formed another new droplet F. It should be noted that the new coalescent droplet in terms of droplets on the front and side surfaces of cold plate may be located on either of front or side surfaces. This is mainly dependent on the combined effect of droplet surface tension and droplet gravity. The droplet coalescence that occurred between the front and side surfaces of the cold plate was also one of the main reasons that resulted in much larger droplets near the plate edge on its front surface than in other regions.

On the other hand, it can be noted that the freezing process of droplets took place in sequence approximately, although no ice bridges between droplets were observed. As shown in Fig. 6(b), the wave red dash line is used for distinguishing frozen and unfrozen droplets and it varied as time passed. The red dash line can be recognized as a freezing wave and its variation as freezing wave propagation. It should be noted that there may exist different freezing front propagation from the plate edge when two or more droplets in the edge-affected zone solidified at the same time due to the randomness of nucleation. However, this phenomenon appeared less frequently in our experiments and the corresponding experiments were eliminated to ensure the uniformity of all the cases. Therefore, there is only one front freezing wave propagation in all the reported cases. Besides, it was also noted

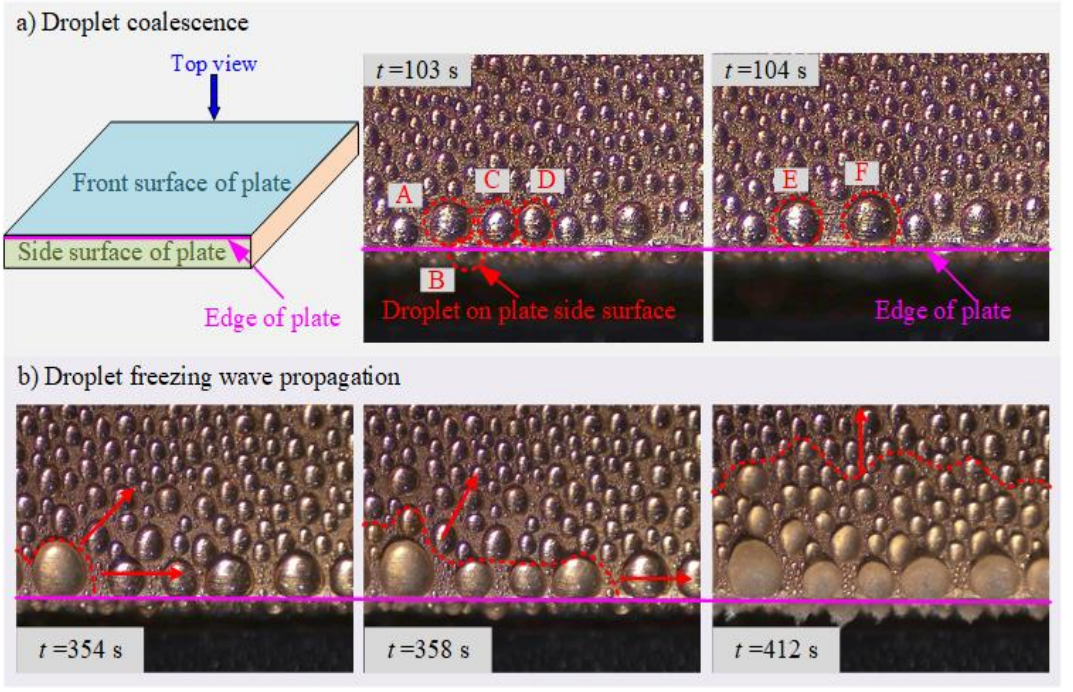

Fig. 6 Schematics of droplet coalescence and freezing wave propagation.

that the freezing process of droplets near the plate edge was much faster than that in other regions. The quantitative analysis will be presented in Section 3.2.

3.2 Droplet size and distribution characteristics

As demonstrated in Section 3.1, the differences in condensation frosting characteristics among different plate temperatures and plate zones were significant. Besides, as mentioned in Section 2.3, the front surface of cold plate was divided into an edge-affected zone and an unaffected zone based on droplet size characteristics. To further quantitatively investigate the effects of plate temperature and plate edge, droplet size and distribution characteristics in edge-affected and unaffected zones for Cases 1 to 5 are presented in this section.

Figure 7 shows the stage periods in edge-affected and unaffected zones for Cases 1 to 5. As seen, the droplet condensation stage periods for Cases 1 and 2 were both larger than 1,200 s and no frozen phenomena were observed. The results demonstrated that droplets may steadily grow up in a supercooled state even though the cold plate temperature was lower to -8.0 °C under the experimental frosting conditions. For Cases 3 to 5, the droplet condensation stage period decreased with a decrease in plate temperature. It was 351 s at a plate temperature of -9.0 °C, and decreased by 69.2% and 88.0% when the plate temperature decreased to -14.0 and -19.0 °C, respectively. The frozen stage period of the edge-affected zone was significantly smaller than that of the unaffected zone. One reason was that the area of the edge-

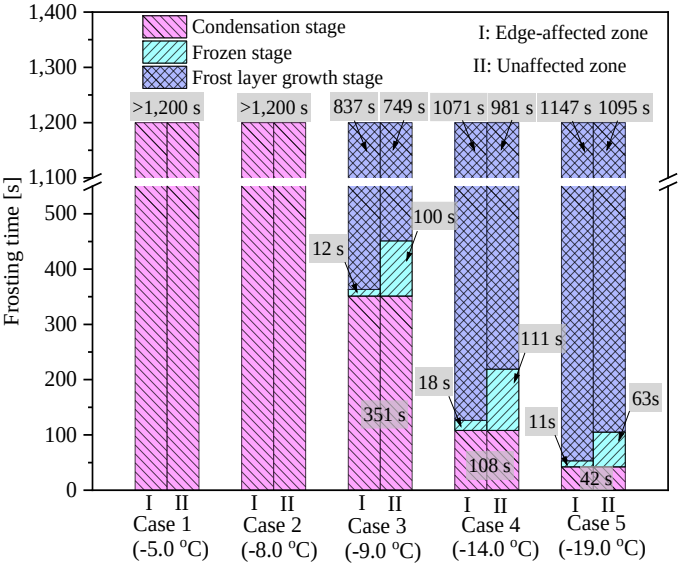

Fig. 7 Stage periods in edge-affected and unaffected zones for Cases 1 to 5.

affected zone was much smaller than that of the unaffected zone. Another reason was that the freezing wave propagation velocity in the edge-affected zone was also smaller than that of the unaffected zone due to their droplet size and distribution characteristics. Besides, it can be found that the droplet frozen stage period did not consistently decrease with a decrease in plate temperature. Generally, the driving force for freezing increased with a decrease in plate temperature. That was why the frozen stage period for Case 5 was significantly smaller than those for Cases 3 and 4. On the other hand, the number of droplets for Case 3 was significantly less than that for Case 4

due to its longer condensation stage, which may reduce the total required time for freezing. As a result, the frozen stage period for Case 4 was slightly larger than that for Case 3. Considering the droplet condensation and frozen stages as the initial frosting stage, its period decreased with a decrease in plate temperature.

To better understand the effect of plat edge on the condensation frosting characteristics of a cold plate, the equivalent width of the edge-affected zone was proposed and evaluated. As shown in Fig. 8, the equivalent width of edge-affected zone is the width of a rectangular which owns the same length and area as those of the edge-affected zone. Therefore, the equivalent width of edge-affected zone can be used for representing the influencing scope of the plate edge effect. Considering the edge-affected zone was zoned in terms of droplets, the equivalent width of the edge-affected zone was only presented during droplet condensation and frozen stages. As seen, the equivalent width of the edge-affected zone for five cases consistently increased as time passed. For Cases 1 and 2, the equivalent width of the edge-affected zone increased to 606.8 × 10^{-6} and 757.8 × 10^{-6} m at 1,200 s, respectively. For Cases 3 to 5, the equivalent width of the edge-affected zone rapidly increased before the droplet frozen stages. At the end of their respective condensation stages, the equivalent width of the edge-affected zone for Cases 3, 4, and 5 were 325.9 × 10^{-6}, 156.4 × 10^{-6} and 90.1 × 10^{-6} m, respectively. Thereafter, these values slightly increased during their respective droplet frozen stages.

Generally, the equivalent width of the edge-affected zone, or the influencing scope of plate edge effect increased with a decrease in plate temperature at the same time before entering into the frost layer growth stage. For example, the equivalent width of the edge-affected zone increased by 5.5% when the plate temperature decreased from -5.0 to -8.0 °C after a 1,200-s droplet condensation period. However, considering the droplet condensation and frozen stages as the initial frosting stage, its period decreased with a decrease in plate temperature. As a result, the equivalent width of the edge-affected zone, or the influencing scope of plate edge effect decreased with a decrease in plate temperature at the end of their respective droplet frozen stages. The equivalent width of the edge-affected zone decreased by 70.8% when the plate temperature decreased from -9.0 to -19.0 °C at the end of their respective droplet frozen stages.

Area-average equivalent diameter of droplets was another important parameter to evaluate droplet size and distribution characteristics. As shown in Fig. 9, the area-average equivalent diameter of droplets for five cases consistently

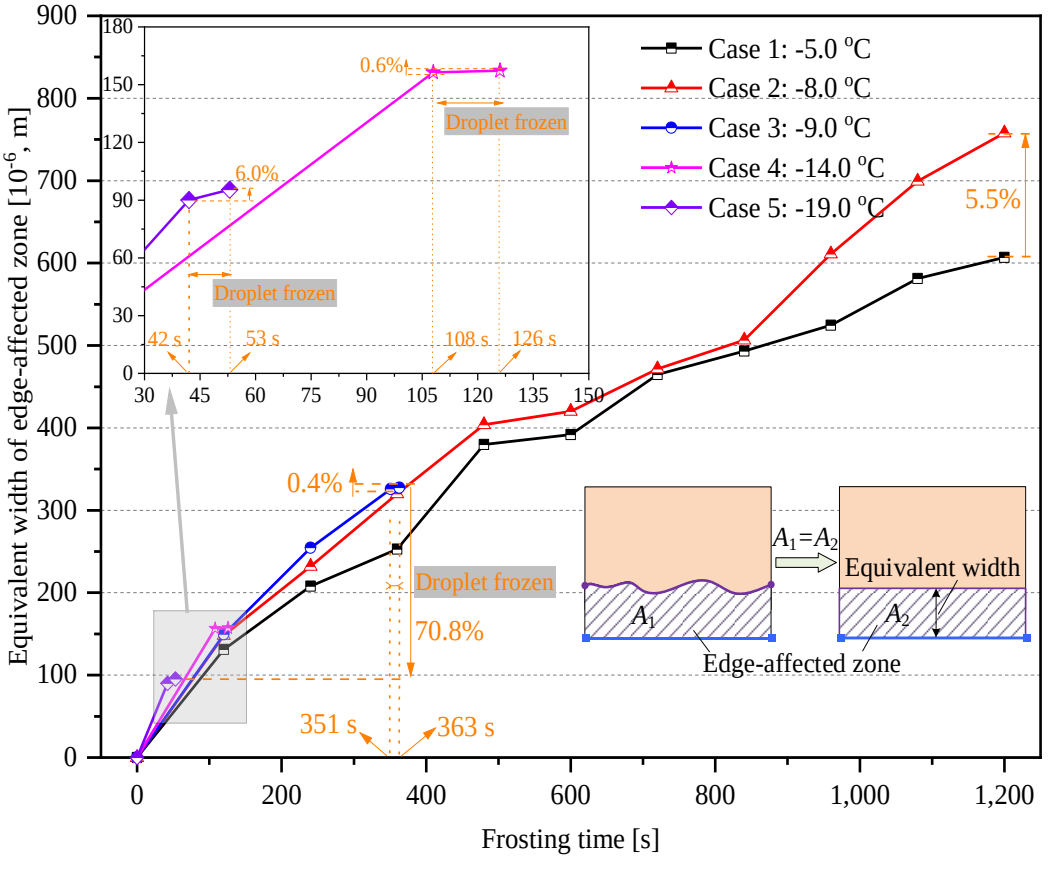

Fig. 8 Equivalent width of the edge-affected zone for Cases 1 to 5.

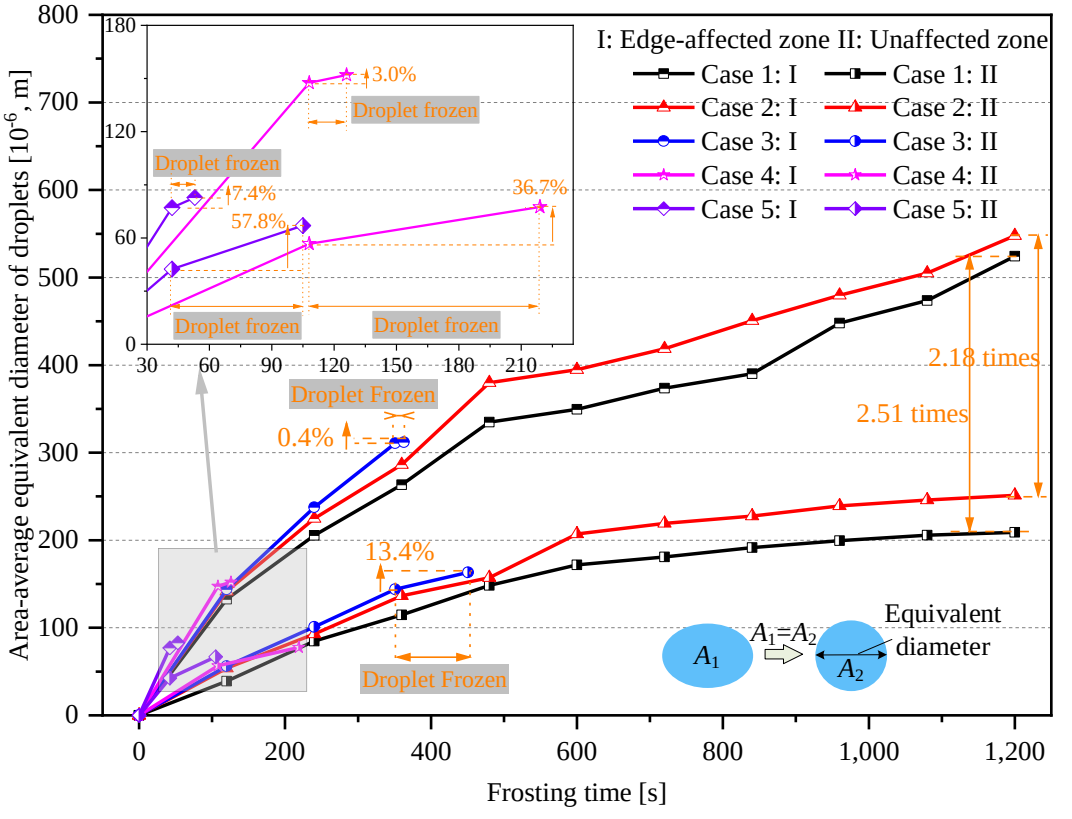

Fig. 9 Area-average equivalent diameter of droplets for Cases 1 to 5.

increased as time passed. For Cases 1 and 2, the area-average equivalent diameter of droplets in the unaffected zones increased to 208.9 × 10^{-6} and 251.2 × 10^{-6} m at 1,200 s, respectively. The corresponding values in edge-affected zones were 2.51 and 2.18 times than those in unaffected zones. For Cases 3 to 5, the area-average equivalent diameter of droplets in both edge-affected and unaffected zones rapidly increased before the droplet frozen stages. At the end of their respective condensation stages, the area-average equivalent diameter of droplets for Cases 3, 4, and 5 were 144.0 × 10^{-6}, 56.7 × 10^{-6} and 42.4 × 10^{-6} m in the unaffected zone, and 310.6 × 10^{-6}, 147.5 × 10^{-6} and 77.1 × 10^{-6} m in the edge-affected zone, respectively. Thereafter, these values increased during their respective droplet frozen stages. In general, the increasing rates in area-average equivalent diameter of droplets in edge-affected zones during droplet frozen stages were significantly lower than that in unaffected zones. This was because the frozen stage periods in edge-affected zones were much shorter than those in unaffected zones and the difference in the contact area of a droplet before and after freezing was slight.

On the one hand, the area-average equivalent diameter of droplets increased with a decrease in plate temperature at the same time before entering into droplet frozen stage. This was because the driving force for condensing increased with a decrease in plate temperature. On the other hand, the area-average equivalent diameter of droplets decreased with a decrease in plate temperature at the end of their respective droplet condensation and frozen stages due to the notable shortened onset time of freezing. Besides, the area-average equivalent diameter of droplets in edge-affected zones was consistently larger than those in the corresponding unaffected zones due to the plate edge effect. At the end of their respective droplet frozen stages, the area-average equivalent diameter of droplets in edge-affected zones at plate temperatures of -9.0, -14.0, and -19.0 °C were 311.8 × 10^{-6}, 152.0 × 10^{-6}, and 82.8 × 10^{-6} m, and 1.91, 1.96 and 1.24 times larger than those in unaffected zones, respectively.

Corresponding to the area-average equivalent diameter of droplets, its average height was also quantified in this study. Since the droplets in the edge-affected zone were larger than those in the unaffected zone, the latter was obscured by the former in terms of the photos captured by the side view camera. Therefore, only the average height of droplets in the edge-affected zone was obtained, as shown in Fig. 10. As seen, the average height of droplets for five cases consistently increased as time passed. For Cases 1 and 2, the average height of droplets in the edge-affected zones increased to 228.4 × 10^{-6} and 336.8 × 10^{-6} m at 1,200 s, respectively. For Cases 3, 4, and 5, the average height of droplets in the edge-affected zones at the end of their respective condensation stages were 164.3

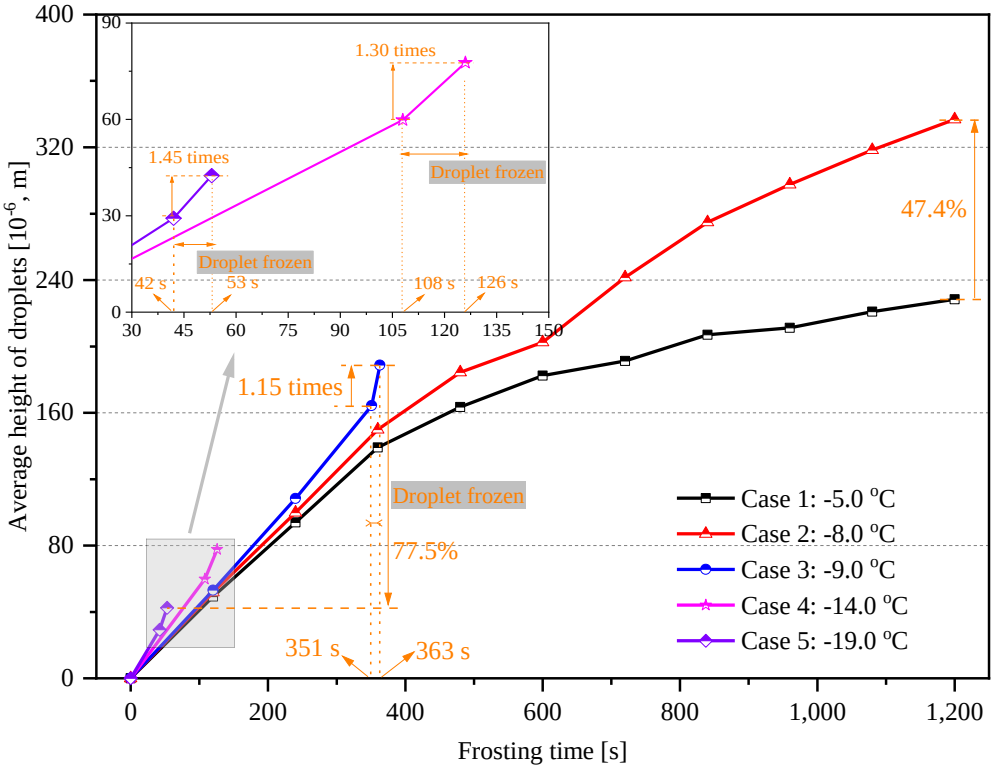

Fig. 10 Average height of droplets in the edge-affected zones for Cases 1 to 5.

$\times 10^{-6}$, 59.8×10^{-6} and 29.2×10^{-6} m, respectively. Thereafter, these values rapidly increased during their respective droplet frozen stages. This was mainly because a notable increase in droplet height would occur before and after its solidification. On the one hand, the average height of droplets increased with a decrease in plate temperature at the same time before entering into droplet frozen stage due to the increased driving force for condensing. For example, the average height of droplets in the edge-affected zone increased by 47.4% when the plate temperature decreased from -5.0 to -8.0 °C after a 1,200-s droplet condensation period. On the other hand, the average height of droplets in the edge-affected zone decreased with a decrease in plate temperature at the end of their respective droplet condensation and frozen stages due to the notable shortened onset time of freezing. The average height of droplets in the edge-affected zone decreased by 77.5% when the plate temperature decreased from -9.0 to -19.0 °C at the end of their respective droplet frozen stages.

The coverage area ratio of droplets was also an important parameter in evaluating droplet size and distribution characteristics. As shown in Fig. 11, the coverage area ratio of droplets for five cases consistently increased as time passed. For Cases 1 and 2, the coverage area ratio of droplets in the unaffected zones increased to 71.5% and 74.2% at 1,200 s, respectively. The corresponding values in edge-affected zones were 10.6% and 9.6% higher than those in unaffected zones. For Cases 3 to 5, the coverage area ratio of droplets in both edge-affected and unaffected zones rapidly increased before the droplet frozen stages. At the end of their respective condensation stages, the coverage area ratio of droplets for Cases 3, 4, and 5 were 64.1%, 49.1%, and 46.6% in the unaffected zone, and 71.5%, 63.0%, and 51.8% in edge-affected zone, respectively. Thereafter, these values increased during their respective droplet frozen stages. Besides, the increasing rates in coverage area ratio of droplets in edge-affected zones during droplet frozen stages were significantly lower than that in unaffected zones. This was because the frozen stage periods in edge-affected zones were much shorter than those in unaffected zones and the difference in the contact area of a droplet before and after freezing was slight. As a result, the coverage area ratio of droplets in the unaffected zone for Case 5 surpassed that in the edge-affected zone at the end of their respective droplet frozen stages.

In general, the coverage area ratio of droplets increased with a decrease in plate temperature at the same time before entering into droplet frozen stage due to the increased driving force for condensing. By contrast, the coverage area ratio of droplets decreased with a decrease in plate temperature at the end of their respective droplet condensation and frozen stages due to the notably shortened onset time of freezing. The coverage area ratio of droplets in the edge-affected and unaffected zones decreased by 19.7% and 10.0% when the plate temperature decreased from -9.0 to -19.0 °C at the end of their respective droplet frozen stages.

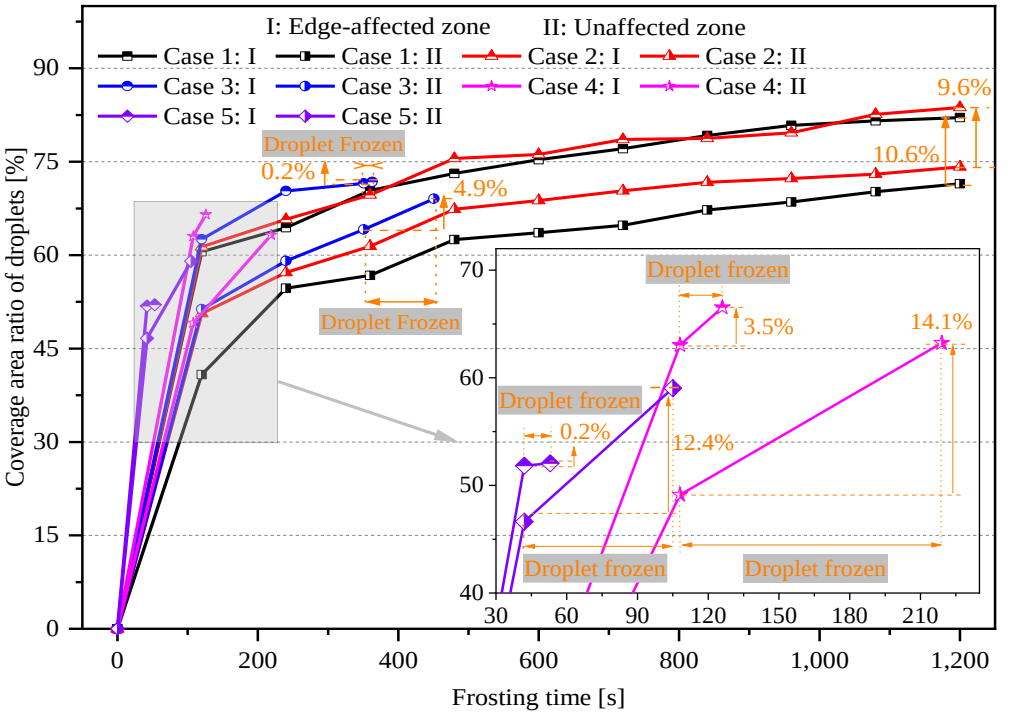

Fig. 11 Coverage area ratio of droplets for Cases 1 to 5.

As mentioned in Section 3.1, an obvious freezing wave propagation can be observed during the droplet frozen stages for Cases 3 to 5. Based on Eq. (4), the average velocity of freezing wave propagation can be roughly evaluated, as shown in Fig. 12. In general, the average freezing wave propagation velocity in edge-affected zones was much larger than those in unaffected zones under the same frosting condition. This was mainly because the diameter and coverage area ratio of droplets in edge-affected zone were much larger than those in unaffected zone, as demonstrated in Figs. 9 and 11. It was

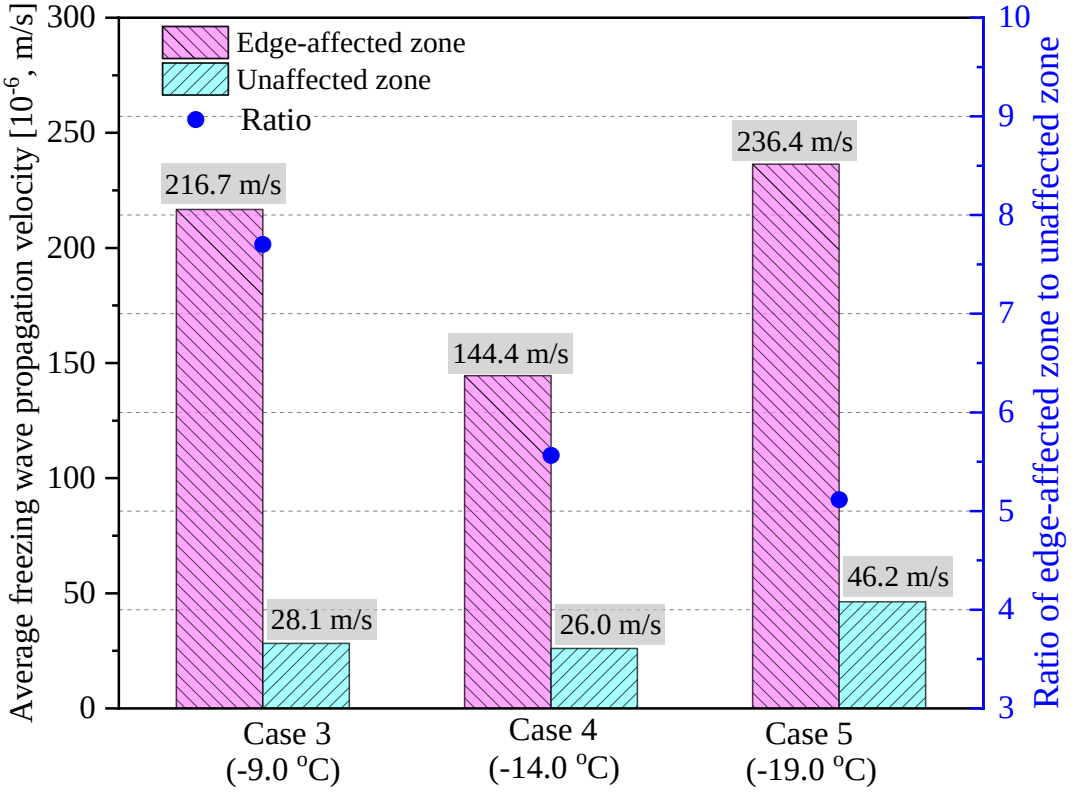

Fig. 12 Average freezing wave propagation velocity for Cases 3 to 5.

noted that one important factor influencing the freezing wave propagation was the distance between droplets. Therefore, larger diameter and coverage area ratio of droplets may result in a shorter distance between droplets, and hence facilitate the freezing wave propagation. The ratio of average freezing wave propagation velocity in edge-affected zone to that in unaffected zone for Cases 3, 4, and 5 at plate temperatures of -9.0, -14.0, and -19.0 °C were 7.70, 5.56, and 5.11, respectively. On the other hand, since the driving force for freezing increased with a decrease in plate temperature, the average freezing wave propagation velocity at a plate temperature of -19.0 °C was much larger than those at plate temperatures of -9.0 and -14.0 °C. However, it can be noted that the average freezing wave propagation velocity at a plate temperature of -14.0 °C was lower than that at -9.0 °C. This was because the diameter and coverage area ratio of droplets of the latter were much larger than those of the former. Considering the diameter and coverage area ratio of droplets increased with a decrease in plate temperature, the average freezing wave propagation velocity was not consistently increased with a decrease in plate temperatures.

3.3 Analysis of frost crystal behaviors

As mentioned in Section 3.2, frost crystals grow in three-dimension and intertwine with each other as time passes. It should be noted that frost crystal growth was a complicated heat and mass transfer process coupled with gravity and aerodynamic force. As shown in Fig. 13, frost crystal sublimation and collapse can be observed by comparing frost crystals in locations A, B, and C at different time points. For location A, it can be seen that a plate-type frost crystal disappeared as time passed. Since no water film was observed during this process, it was believed that the plate-type frost crystal sublimated and the corresponding water vapor was absorbed by its surrounding frost crystals. When the sublimation occurred at the bottom of a frost crystal and the puny local part of the frost crystal was not strong enough to support the upper frost crystal, the upper frost crystal would collapse under the action of gravity and aerodynamic force. For example, frost crystals in locations B and C in Fig. 13 collapsed in the direction of air flow due to the sublimation of their bottom part. In general, simple frost crystal sublimation can be recognized as a kind of heat and mass transfer between frost crystals, and may not affect the growth process of frost layer notably. However, frost crystal collapse resulting from sublimation may affect the growth process of frost layer to some extent, which may facilitate the growth in frost layer density but impede the growth in frost layer thickness. Whereas all the existing frosting models did not consider frost crystal collapse, the relevant studies should be further investigated.

3.4 Frost layer growth characteristics

As demonstrated in Section 3.1, the frosting process in the edge-affected zone was much faster than that in the unaffected zone. Therefore, the frost layer in unaffected zone may be obscured by that in the edge-affected zone in terms of the photos captured by the side view camera. As a result, similar to the average height of droplets, only the frost layer growth characteristics such as thickness, growth rate, and surface roughness in the edge-affected zone, are presented in this section.

Frost layer thickness is one of the most important frosting characteristic parameters and usually used for evaluating the level of frosting in practical applications. For example, the blockage ratio of outdoor coil of an air source heat pump is evaluated by frost layer thickness and can indicate the blocking degree in air passage of outdoor coil by frosting. As shown in Fig. 14, frost layer thickness for Cases 3 to 5 consistently increased as time passed and it increased with a decrease in plate temperature at the same time point. At 1,200 s, the frost layer thickness for Case 3 at a plate temperature of

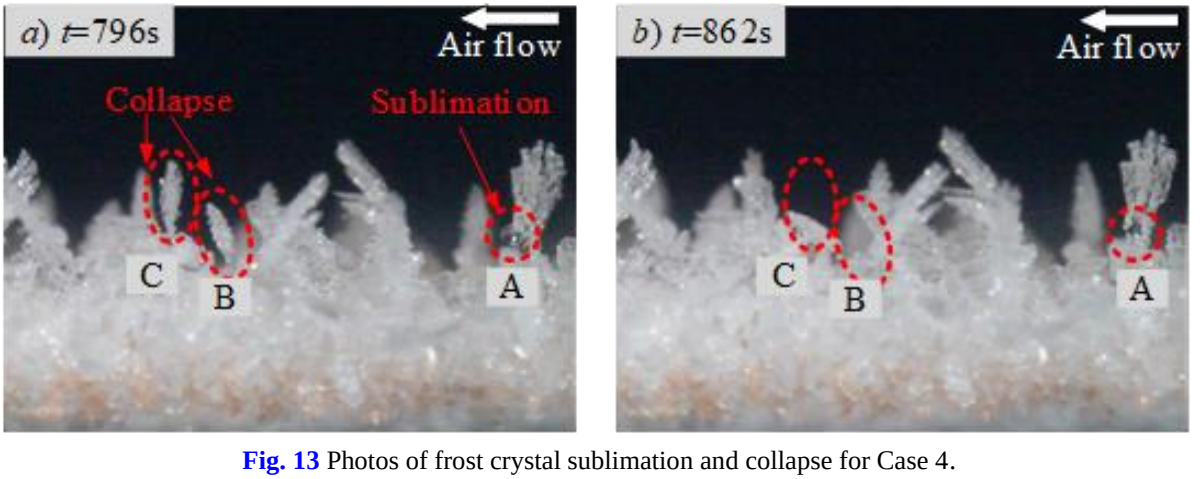

Fig. 13 Photos of frost crystal sublimation and collapse for Case 4.

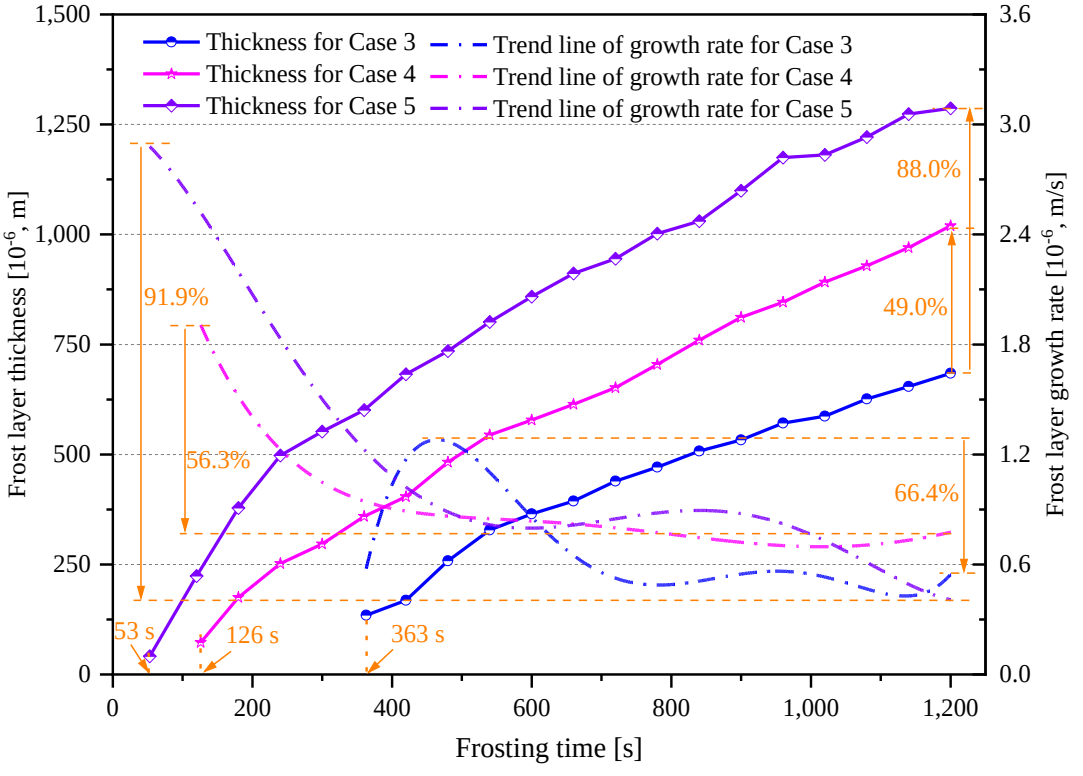

Fig. 14 Frost layer thickness and growth rate in edge-affected zones for Cases 3 to 5.

-9.0 °C was 684.4 × 10^{-6} m, and it increased by 49.0% and 88.0%, respectively, when the plate temperature decreased to -14.0 and -19.0 °C. Besides, the initial frost layer thickness for Cases 3, 4, and 5 at the start of their respective frost layer growth stages were 134.7 × 10^{-6}, 72.8 × 10^{-6}, and 41.2 × 10^{-6} m, respectively. It can be noted that the initial frost layer thickness decreased with a decrease in plate temperature due to the notably shortened droplet condensation and frozen stages.

On the other hand, the frost layer growth rate can be evaluated based on the time variations of frost layer thickness. Considering the random growth characteristic of frost crystal and the collapse of frost crystal, the frost layer growth rate dramatically fluctuated during the frosting period. To avoid cluttered data points, Fig. 14 only presents the trend line of frost layer growth rate for Cases 3 to 5. As seen, the initial frost layer growth rate increased with a decrease in plate temperature, but the overall reduction rate in frost layer growth rate also increased with a decrease in plate temperature. For Cases 4 and 5, the frost layer growth rate gradually decreased as time passed due to the consistently increased frost layer surface temperature. By contrast, the frost layer growth rate for Case 3 increased firstly and then decreased as time passed. This was because the initial frost crystals for Case 3 were much sparse due to the large droplets and can provide conditions for the rapid growth of frost crystals. In general, it can be inferred that the initial droplet size and distribution characteristics may notably affect frost crystal growth at the early frost layer growth stage. At 1,200 s, the frost layer growth rate for Cases 3, 4, and 5 were 66.4%, 56.3%, and 91.9% lower than their respective maximum values during frost layer growth stages.

Frost layer surface roughness was a characteristic parameter used for evaluating frost layer morphology. As shown in Fig. 15, similar to frost layer growth rate, frost layer surface roughness dramatically fluctuated due to the random growth characteristic of frost crystal and collapse of frost crystal. Overall, frost layer surface roughness gradually increased as time passed. At the start of the frost layer growth stage, frost layer surface roughness was mainly dependent on droplet size and distribution characteristics. As a result, the initial frost layer surface roughness decreased with a decrease in plate temperature. Thereafter, frost layer surface roughness rapidly increased due to the uneven growth of frost crystals. It can be noted that frost layer surface roughness for Case 5 lowered than that for Case 4 at the later frost layer growth stage. This was mainly because the frost surface temperature for Case 5 rapidly increased due to its rapidly increased frost layer thickness. The higher frost surface temperature may lead to a denser frost layer and hence a smaller frost layer surface roughness. Therefore, the relationship between frost layer surface roughness and plate temperature was nonlinear and may change as frosting progressed. At 1,200 s, the frost layer surface roughness for Cases 3, 4, and 5 were 70.9 × 10^{-6}, 106.5 × 10^{-6}, 100.8 × 10^{-6} m, and 40.8%, 8.4 times, and 9.0 times larger than their initial values during frost layer growth stages.

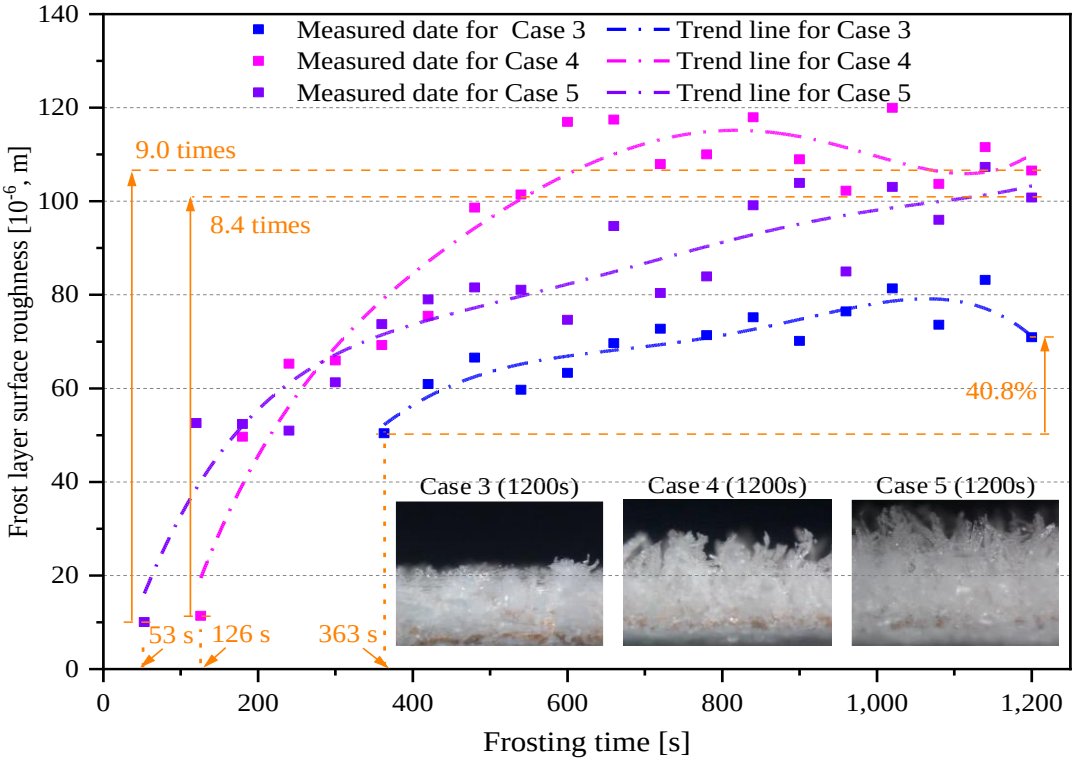

Fig. 15 Frost layer surface roughness in edge-affected zones for Cases 3 to 5.

4. Conclusions

In terms of the plate edge effect, the droplet size and distribution, and frost layer growth characteristics at the early condensation frosting stage are experimentally investigated under different plate temperatures. The main conclusions of this study can be made as follows:

1. Under the experimental conditions, droplets may steadily grow up in a supercooled state even though the cold plate temperature was lowered to -8.0 ºC. As the plate temperature continued to decrease, droplet frozen and frost layer growth stages may occur. The droplet condensation stage period was 351 s at a plate temperature of -9.0 ºC, and decreased by 69.2% and 88.0% when the plate temperature decreased to -14.0 and -19.0 ºC, respectively.

2. The frozen stage period of the edge-affected zone was significantly smaller than that of the unaffected zone. The ratio of average freezing wave propagation velocity in edge-affected zone to that in the unaffected zone at plate temperatures of -9.0, -14.0, and -19.0 ºC were 7.70, 5.56, and 5.11, respectively. Besides, the droplet frozen stage period and average freezing wave propagation velocity did not consistently decrease with a decrease in plate temperature, although the driving force for freezing increased. The sum of droplet condensation and frozen stage periods decreased with a decrease in plate temperature.

3. At the same time point, the influencing scope of plate edge effect increased with a decrease in plate temperature. The equivalent width of the edge-affected zone increased by 5.5% when the plate temperature decreased from -5.0 to -8.0 ºC after a 1,200-s droplet condensation period. By contrast, at the end of their respective droplet condensation stages, the influencing scope of plate edge effect decreased with a decrease in plate temperature. The equivalent width of the edge-affected zone decreased by 70.8% when the plate temperature decreased from -9.0 to -19.0 ºC.

4. The area-average equivalent diameter and coverage area ratio of droplets decreased with a decrease in plate temperature at the end of their respective droplet frozen stages. At the end of droplet frozen stages, the area-average equivalent diameter of droplets in edge-affected zones at plate temperatures of -9.0, -14.0, and -19.0 ºC were 311.8×10^{-6}, 152.0×10^{-6}, and 82.8×10^{-6} m, and 1.91, 1.96 and 1.24 times larger than those in unaffected zones, respectively. The coverage area ratio of droplets in the edge-affected and unaffected zones decreased by 19.7% and 10.0% when the plate temperature decreased from -9.0 to -19.0 ºC.

5. The initial frost layer thickness decreased with a decrease in plate temperature due to the shortened droplet condensation and frozen stages. At 1,200 s, the frost layer thickness at a plate temperature of -9.0 ºC was 684.4×10^{-6} m, and increased by 49.0% and 88.0% when the plate temperature decreased to

-14.0 and -19.0 °C. Besides, the relationship between frost layer surface roughness and plate temperature was nonlinear and may vary as frosting progressed. At 1,200 s, the frost layer surface roughness at plate temperatures of -9.0, -14.0, and -19.0 °C were 70.9 × 10^{-6}, 106.5 × 10^{-6}, and 100.8 × 10^{-6} m, respectively.

Acknowledgments

The corresponding author acknowledges the financial supports from the National Natural Science Foundation of China (Grant No. 52076013), Beijing Municipal Science & Technology Commission (Grant No. 3212024), Open Fund of Key Laboratory of Icing and Anti/De-icing (Grant No. IADL20200104), and the CAS Key Laboratory of Cryogenics, Technical Institute of Physics and Chemistry, China (Grant No. CRYO202001, Grant No. CRYO202104), and National Natural Science Foundation of China (Grant No. 51925605).

Conflict of Interest

There is no conflict of interest.

Supporting Information

Not applicable.

Nomenclature

A	area [m^2]
$\bar{D}$	area-average equivalent diameter [m]
g	growth rate [m/s]
H	droplet height [m]
$\bar{H}$	average droplet height [m]
L	equivalent distance in the corresponding zone [m]
N	number [-]
p_v	vapor partial pressure of the humid air [Pa]
p_s	saturated vapor pressure at the cold plate temperature [Pa]
R_A	coverage area ratio of droplets [%]
R_w	gas constant for water vapor [J/(kg·K)]
RMS	root-mean-square roughness [m]
T_v	vapor temperature [K]
u	uncertainty [%]
v	velocity [m/s]
Greek symbols	
σ_{vl}	interfacial free energy between vapor and liquid [N/m]
δ	thickness [m]
$\bar{\delta}$	average thickness [m]
ρ_l	liquid water density [kg/m^3]
θ	surface contact angle [°]
Δt	duration of frozen stage [s]
$\Delta t'$	time interval used for measuring frost thickness [s]
ΔG_c	heterogeneous nucleation energy barrier [J]
Subscripts	
f	frost
fw	freezing wave
p	pixel
p, in	pixels inside a water droplet
sp	sampling points
s	surface of the corresponding zone
w	Water

References

[1] I. Hůnová, M. Novák, P. Kurfürst, H. Škáchová, M. Štěpánová, E. Přechová, A. Komárek, J. Čuřík, F. Veselovský, L. Bohdálková, Contribution of rime to atmospheric sulphur deposition in Central Europe: A combined empirical and modelling approach, *Atmospheric Environment*, 2022, **270**, 118877, doi: 10.1016/j.atmosenv.2021.118877.

[2] J. Koszut, K. Boyina, G. Popovic, J. Carpenter, S. Wang, N. Miljkovic, Superhydrophobic heat exchangers delay frost formation and reduce defrost energy input of aircraft environmental control systems, *International Journal of Heat and Mass Transfer*, 2022, **189**, 122669, doi: 10.1016/j.ijheatmasstransfer.2022.122669.

[3] Z. Liu, Y. Hu, X. Jiang, Y. Wu, M. Chi, F. Han, X. Wang, Three-dimensional numerical simulation of rime ice accumulation on silicone rubber insulator and its experimental verification in the natural environment, *Electric Power Systems Research*, 2022, **213**, 108713, doi: 10.1016/j.epsr.2022.108713.

[4] D. Badri, C. Toublanc, O. Rouaud, M. Havet, Review on frosting, defrosting and frost management techniques in industrial food freezers, *Renewable and Sustainable Energy Reviews*, 2021, **151**, 111545, doi: 10.1016/j.rser.2021.111545.

[5] L. Zhang, M. J. Song, S. H. Hosseini, J. Shen, Y. Q. Jiang, A modeling study of spatial and temporal frost growth on the edge of windward fins for a tube-finned heat exchanger, *International Journal of Heat and Mass Transfer*, 2022, **183**, 122093, doi: 10.1016/j.ijheatmasstransfer.2021.122093.

[6] L. Zhang, M. J. Song, N. Mao, J. K. Dong, Temporal and spatial frost growth prediction of a tube-finned heat exchanger considering frost distribution characteristics, *International Journal of Heat and Mass Transfer*, 2022, **183**, 122192, doi: 10.1016/j.ijheatmasstransfer.2021.122192.

[7] Y. A. Andrade-Ambriz, S. Ledesma, J. M. Belman-Flores, I. Carvajal-Mariscal, D.-L. Almanza-Ojeda, Frost thickness estimation in a domestic refrigerator using acoustic signals and artificial intelligence, *Expert Systems with Applications*, 2022, **201**, 117071, doi: 10.1016/j.eswa.2022.117071.

[8] F. Wang, C. Liang, X. Zhang, Research of anti-frosting technology in refrigeration and air conditioning fields: a review, *Renewable and Sustainable Energy Reviews*, 2018, **81**, 707-722, doi: 10.1016/j.rser.2017.08.046.

[9] X. Bai, S. Liu, S. Deng, L. Zhang, M. Wei, An experimental study on achieving even-frosting for an air source heat pump using a novel dual-fan outdoor coil, *Energy and Buildings*, 2022, **255**, 111695, doi: 10.1016/j.enbuild.2021.111695.

[10] L. Zhang, Y. Jiang, J. Dong, Y. Yao, S. Deng, An experimental study of frost distribution and growth on finned tube heat exchangers used in air source heat pump Applied Thermal Engineering units, *Applied Thermal Engineering*, 2018, **132**, 38-51, doi: 10.1016/j.applthermaleng.2017.12.047.

[11] S. Byun, H. Jeong, D. R. Kim, K.-S. Lee, Frost layer growth behavior on ultra-low temperature surface with a superhydrophobic coating, *International Communications in Heat and Mass Transfer*, 2021, **128**, 105641, doi: 10.1016/j.icheatmasstransfer.2021.105641.

[12] R. Tang, F. Wang, Z. Wang, W., Division of frosting type and frosting degree of the air source heat pump for heating in china, *Frontiers in energy research*, 2021, **9**, 708478, doi: 10.3389/fenrg.2021.708478.

[13] L. Zhang, M. Song, S. Deng, J. Shen, C. Dang, Frosting mechanism and behaviors on surfaces with simple geometries: a state-of-the-art literature review, *Applied Thermal Engineering*, 2022, **215**, 118984, doi: 10.1016/j.applthermaleng.2022.118984.

[14] J.-T. Kwon, D.-H. Kim, C. Huh, S. Koyama, Y.-C. Kwon, Frost distribution characteristics of laminar airflow on cold surface of mini-channels, *International Communications in Heat and Mass Transfer*, 2011, **38**, 887-892, doi: 10.1016/j.icheatmasstransfer.2011.04.007.

[15] H. Ramírez-Hernández, F. Sánchez-Cruz, F. Solorio-Ordaz, S. Martínez-Martínez, An experimental study of heat transfer on a tube bank under frost formation conditions, *International Journal of Refrigeration*, 2091, **102**, 35-40, doi: 10.1016/j.ijrefrig.2019.01.031.

[16] V. S. Nascimento Jr, F. R. Loyola, C. J. L. Hermes, A study of frost build-up on parallel plate channels, *Experimental Thermal and Fluid Science*, 2015, **60**, 328-336, doi: 10.1016/j.expthermflusci.2014.10.006.

[17] X. Wu, S. Hu, F. Chu, Experimental study of frost formation on cold surfaces with various fin layouts, *Applied Thermal Engineering*, 2016, **95**, 95-105, doi: 10.1016/j.applthermaleng.2015.11.045.

[18] A. Léoni, M. Mondot, F. Durier, R. Revellin, P. Haberschill, State-of-the-art review of frost deposition on flat surfaces, *International Journal of Refrigeration*, 2016, **68**, 198-217, doi: 10.1016/j.ijrefrig.2016.04.004.

[19] C. Cheng, C. Shiu, Frost formation and frost crystal growth on a cold plate in atmospheric air flow, *International Journal of Heat and Mass Transfer*, 2002, **45**, 4289-4303, doi: 10.1016/S0017-9310(02)00134-5.

[20] W. Wang, Q. C. Guo, W. P. Lu, Y. C. Feng, W. Na, A generalized simple model for predicting frost growth on cold flat plate, *International Journal of Refrigeration*, 2012, **35**, 475-486, doi: 10.1016/j.ijrefrig.2011.10.011.

[21] C. J. L. Hermes, R. O. Piucco, J. R. Barbosa Jr, C. Melo, A study of frost growth and densification on flat surfaces, *Experimental Thermal and Fluid Science*, 2009, **33**, 371-379, doi: 10.1016/j.expthermflusci.2008.10.006.

[22] Y. Lee, S. Ro, Analysis of the frost growth on a flat plate by simple models of saturation and supersaturation, *Experimental Thermal and Fluid Science*, 2005, **29**, 685-696, 10.1016/j.expthermflusci.2004.11.001.

[23] J. Y. Gong, J. J. Sun, G. J. Li, An experimental study of the effect of air quality on frosting on cold flat surface, *International Communications in Heat and Mass Transfer,* 2017, **82**, 139-144, doi: 10.1016/j.icheatmasstransfer.2017.02.013.

[24] V. Tudor, M. Ohadi, The effect of stationary and sweeping frequency AC electric fields on frost crystal removal on a cold plate, *International Journal of Refrigeration*, 2006, **29**, 669-677, doi: 10.1016/j.ijrefrig.2005.08.015.

[25] Y. Qin, B. Dong, W. Li, Experimental study of the frosting characteristic of water on a cold surface in the magnetic field, *Experimental Thermal and Fluid Science*, 2020, **114**, 110044, doi: 10.1016/j.expthermflusci.2020.110044.

[26] A. Chen, Y. Meng, B. Liu, Y. Li, Z. Miao, Effects of inclination on the frosting process on cold surface of copper heat exchanger, *Energy and Buildings*, 2021, **231**, 110628, doi: 10.1016/j.enbuild.2020.110628.

[27] J. Kim, S. Byun, J. Lee, K. Lee, Frost growth behavior according to the cold surface inclination angle, *International Journal of Heat and Mass Transfer*, 2020, **146**, 118841, doi: 10.1016/j.ijheatmasstransfer.2019.118841.

[28] C. J. L. Hermes, V. S. Nascimento, F. R. Loyola, R. P. Cardoso, A. D. Sommers, A study of frost build-up on hydrophilic and hydrophobic surfaces under forced convection conditions, *Experimental Thermal and Fluid Science*, 2019, **100**, 76-88, doi: 10.1016/j.expthermflusci.2018.08.009.

[29] H. Kim, D. Kim, H. Jang, D. R. Kim, K.-S. Lee, Microscopic observation of frost behaviors at the early stage of frost formation on hydrophobic surfaces, *International Journal of Heat and Mass Transfer*, 2016, **97**, 861-867, doi: 10.1016/j.ijheatmasstransfer.2016.02.020.

[30] W. Sheng, Y. Pei, X. Li, P. Ming, W. Zhao, Effect of surface characteristics on condensate droplets growth, *Applied Thermal Engineering*, 2020, **173**, 115260, doi: 10.1016/j.applthermaleng.2020.115260.

[31] A. Ashrafi-Habibabadi, A. Moosavi, Droplet condensation and jumping on structured superhydrophobic surfaces, *International Journal of Heat and Mass Transfer*, 2019, **134**, 680-693, doi: 10.1016/j.ijheatmasstransfer.2019.01.026.
[32] X. Wu, W. Dai, W. Xu, L. Tang, Mesoscale investigation of frost formation on a cold surface, *Experimental Thermal and Fluid Science*, 2007, **31**, 8, 1043-1048, doi: 10.1016/j.expthermflusci.2006.11.002.
[33] M. Lu, M. Song, X. Pang, C. Dang, L. Zhang, Modeling study on sessile water droplet during freezing with the consideration of gravity, supercooling, and volume expansion effects, *International Journal of Multiphase Flow*, 2022, **147**, 103909, doi: 10.1016/j.ijmultiphaseflow.2021.103909.
[34] X. Chen, R. Ma, H. Zhou, X. Zhou, L. Che, S. Yao, Activating the microscale edge effect in a hierarchical surface for frosting suppression and defrosting promotion, *Scientific Reports*, 2013, **3**, 1-8, doi: 10.1038/srep02515.
[35] J. B. Boreyko, C. P. Collier, Delayed frost growth on jumping-drop superhydrophobic surfaces, *ACS Nano*, 2013, **7**, 1618-1627, doi: 10.1021/nn3055048.
[36] Y. Zhao, C. Yang, Frost spreading on microscale wettability/morphology patterned surfaces, *Applied Thermal Engineering*, 2017, **121**, 136-145, doi: 10.1016/j.applthermaleng.2017.04.063.
[37] T. Zhang, D. L. O'Neal, S. T. McClain, Impact of environmental conditions on frost crystal structure, *International Journal of Air-Conditioning and Refrigeration*, 2020, **28**, 2050014, doi: 10.1142/s2010132520500145.
[38] M. Song, S. Lei, S. H. Hosseini, X. Luo, Z. Wang, An experimental study on the effect of horizontal cold plate surface temperature on frosting characteristics under natural convection, *Applied Thermal Engineering*, 2022, **211**, 118416, doi: 10.1016/j.applthermaleng.2022.118416.
[39] S. Lei, M. Song, C. Dang, Y. Xu, K. Shao, Experimental study on the effect of surface temperature on the frost characteristics of an inverted cold plate under natural convection, *Applied Thermal Engineering*, 2022, **211**, 118470, doi: 10.1016/j.applthermaleng.2022.118470.
[40] M. J. Song, C. B. Dang, Review on the measurement and calculation of frost characteristics, *International Journal of Heat and Mass Transfer*, 2018, **124**, 586-614, doi: 10.1016/j.ijheatmasstransfer.2018.03.094.
[41] J. Guadarrama-Cetina, A. Mongruel, W. González-Viñas, D. Beysens, Percolation-induced frost formation, *Europhysics letters*, 2013, **101**, 1, 16009, doi: 10.1209/0295-5075/101/16009.
[42] M. R. Haque, S. R. Das, A. R. Betz, Experimental investigation of condensation and freezing phenomena on hydrophilic and hydrophobic graphene coating, *Applied Thermal Engineering*, 2019, **160**, 113987, doi: 10.1016/j.applthermaleng.2019.113987.
[43] M. R. Haque, C. Qu, E. C. Kinzel, A. R. Betz, Droplet growth dynamics during atmospheric condensation on nanopillar surfaces, *Nanoscale and Microscale Thermophysical Engineering*, 2018, **22**, 270-295, doi: 10.1080/15567265.2018.1495282.
[44] M. R. Haque, A. R. Betz, Frost formation on aluminum and hydrophobic surfaces, *International Conference on Nanochannels, Microchannels, and Minichannels*, American Society of Mechanical Engineers, 2018, doi: 10.1115/ICNMM2018-7609.
[45] S. Jung, M. K. Tiwari, D. Poulikakos, Frost halos from supercooled water droplets, *Proceedings of the National Academy of Sciences of the United States of America*, 2012, **109**, 16073-16078, doi: 10.1073/pnas.1206121109.
[46] G. Graeber, V. Dolder, T. M. Schutzius, D. Poulikakos, Cascade freezing of supercooled water droplet collectives, *ACS Nano*, 2018, **12**, 11274-11281, doi: 10.1021/acsnano.8b05921.
[47] L. Zhang, M. J. Song, C. Y. H. Chao, C. B. Dang, J. Shen, Localized characteristics of the first three typical condensation frosting stages in the edge region of a horizontal cold plate, *Micromachines*, 2022, **13**, 1906, doi: 10.3390/mi13111906.
[48] L. Zhang, M. J. Song, C. Y. H. Chao, J. Shen, An experimental study on the dynamic frosting characteristics on the edge zone of a horizontal copper plate under forced convection, *International Journal of Heat and Mass Transfer*, 2023, **200**, 123541, doi: 10.1016/j.ijheatmasstransfer.2022.123541.
[49] S. B. Rasul, A. Monsur Kajal, A. H. Khan, Quantifying uncertainty in analytical measurements, *Journal of Bangladesh Academy of Sciences*, 2018, **41**, 145-163, doi: 10.3329/jbas.v41i2.35494.
[50] X. Wu, W. Dai, X. Shan, W. Wang, L. Tang, Visual and theoretical analyses of the early stage of frost formation on cold surfaces, *Journal of Enhanced Heat Transfer*, 2007, **14**, 257-268, doi: 10.1615/jenhheattransf.v14.i3.70.

Author Information

Long Zhang *is currently an assistant professor in the Department of Energy and Power Engineering, School of Mechanical Engineering, Beijing Institute of Technology, China. He obtained his bachelor's and master's degrees from the Harbin Institute of Technology in 2012 and 2014, respectively. Then, he obtained his doctor's degree in engineering from the Harbin Institute of Technology and doctor's degree in philosophy from the Hong Kong Polytechnic University in 2020 through Joint PhD*

Program. After that, he joined the Department of Energy and Power Engineering at the Beijing Institute of Technology as a Postdoctoral Fellow. His research focuses on the frosting/icing mechanism on cold plates, frosting and aerodynamic characteristics of heat exchangers, and key defrosting technologies of air source heat pumps.

Prof. Mengjie Song *currently services in the Department of Energy and Power Engineering, School of Mechanical Engineering, Beijing Institute of Technology, China. He was educated in Hunan University, Harbin Institute of Technology, and Hong Kong Polytechnic University. He had short work experiences in Guangdong University of Technology, Nanyang Technological University, and The University of Tokyo. In 2019, he built the Frost lab and lead it as the Director. He got the DECRA funding in University of Wollongong in 2020. His research focuses on the coupling mechanism and application of heat and mass transfer and flow, such as frosting, icing, boiling and advanced cooling technologies.*

Tianzhuo Zhan *is an Associate Professor in Toyo University in Japan. He received his B.E. and M.E. degrees from Beihang University and the PhD degree from Kyushu University. He joined National Institute for Materials Science in Japan and Waseda University as a postdoctoral researcher. His research focuses on nanoscale thermal transport and its applications in thermoelectric energy harvesting and thermal management of semiconductor devices.*

Prof. Jun Shen *currently services in the Department of Energy and Power Engineering, School of Mechanical Engineering, Beijing Institute of Technology, China. In 2019, she was funded by the Chinese National Science Foundation Project for Outstanding Young People. Her research focuses on the fundamental and applied investigations of new refrigeration and extremely low-temperature technology. She is also the deputy editor of Applied Thermal Engineering, the vice Chairman of the Rare Earth Magnetic Refrigeration Materials and Technology Committee of the Chinese Society of Rare Earth, and a member of the Cryogenic Committee of the Chinese Society of Refrigeration.*

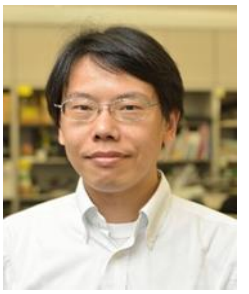

Chaobin Dang *is an Associate Professor in Graduate School of Engineering, University of Fukui in Japan. He received his B.E. and M.E. degrees from Beihang University and the PhD degree from the University of Tokyo. Before the current position, he worked in the University of Tokyo from 2005 to 2021. His research focuses on thermal engineering, heat transfer engineering, air conditioning and refrigeration engineering.*